Achieving Giant Magnetically Induced Reorientation of Martensitic Variants in Magnetic Shape-Memory Ni-Mn-Ga Films by Microstructure Engineering

WILEY-VCH

DOI: 10.1002/((please add manuscript number))
Article type: Communication

Achieving giant magnetically induced reorientation of martensitic variants in magnetic shape memory Ni-Mn-Ga films by microstructure engineering

*Paolo Ranzieri, Marco Campanini, Simone Fabbrici, Lucia Nasi, Francesca Casoli, Riccardo Cabassi, Vincenzo Grillo, Cesar Magén, Federica Celegato, Gabriele Barrera, Paola Tiberto, Franca Albertini**

Dr. P. Ranzieri, Dr. M. Campanini, Dr. S. Fabbrici, Dr. L. Nasi, Dr. F. Casoli, Dr. R. Cabassi, Dr. V. Grillo, Dr. F. Albertini
IMEM-CNR, Parco Area delle Scienze 37/A, Parma, 43124, Italy
E-mail: franca.albertini@imem.cnr.it
Dr. F. Celegato, Dr. G. Barrera, Dr. P. Tiberto
Strada delle Cacce 91, Torino, 10135, Italy
Dr. C. Magén
Instituto de Nanociencia de Aragón, Campus Río Ebro, Calle Mariano Esquillor, 50018 Zaragoza, Spain

Keywords: ferromagnetic shape memory thin films, magnetically induced twin variant reorientation, martensitic microstructure, electron holography, multifunctional magnetic materials

Magnetic shape memory alloys, such as Ni_2MnX (X=Ga, In, Sn, Sb), are multifunctional materials [1,2,3,4,5], with a great potential for the fabrication of microdevices based on novel actuation and sensing mechanisms.[6,7] Giant strains, one order of magnitude higher than the typical magnetostriction and state-of-the-art piezoelectric values, can be obtained by a magnetomechanical effect based on twin variant reorientation induced by magnetic field (MIR). Furthermore, the possibile exploitation of the martensitic distorsions to create tiny machines while keeping simple design[8] and high actuation frequencies makes them particularly appealing for the integration in active microsystems.[9]

Twin variant reorientation was firstly observed and well-assessed in bulk materials[10], where a direct evidence of strains up to 12% in moderate magnetic fields was reported.[11] In the last years a great effort has been done in the investigation of constrained epitaxial thin films grown on different substrates, (i.e. MgO, STO, YSZ)[12-14] and free-standing films.[15-117]

Despite that, very limited MIR effects were found and, although demonstrated, a full comprehension and exploitation of the effect is still lacking. The martensitic microstructure was found to be affected principally by thickness[18,19] and composition[19,20] and a variety of different microstructural and magnetic patterns were obtained. However the role of the martensitic microstructure in determining the MIR has not been fully understood, yet.

In this work, we demonstrate that microstructure can be finely tuned and MIR effect can be accordingly enhanced or suppressed. In particular a giant reversible MIR effect characterized by huge magnetization jumps (up to 55%) is reached in 200 nm thick epitaxial films. Remarkably, such an effect is also dependent on the applied field direction. To deeply investigate its origin, the interplay between crystal structure, orientation and twinning microstrucutre has been established by a multiscale approach, taking advantage of several experimental techniques, including high resolution electron microscopy, electron holography and in-field magnetic force microscopy. In the light of the obtained results, we will demonstrate that the MIR effect in constrained films can be controlled in intensity and anisotropic response by the large scale arrangement of the microstructural twinning patterns.

Films of $Ni_{53,7}Mn_{22.1}Ga_{24.2}$ of thickness 200 nm were grown at T= 350 °C in the austenitic phase on MgO (001) single crystal substrates on top of a 50 nm Cr underlayer. The epitaxial relationships, verified by TEM analysis, are $(001)[100]_{Ni\text{-}Mn\text{-}Ga}$// $(001)[100]_{Cr}$// $(001)[110]_{MgO}$ and $(001)[010]_{Ni\text{-}Mn\text{-}Ga}$// $(001)[010]_{Cr}$// $(001)[-110]_{MgO}$. The martensitic transformation from high temperature cubic austenite into low temperature monoclinic martensite occurs at T=320 K, as shown by resistivity measurements (supplementary information). The crystal structure of the martensite is compatible with the 7M modulated monoclinic structure reported for bulk samples of similar composition.[21] The measured lattice parameters are *a'*= 4.23 Å, *b'*=5.52 Å, *c'* = 4.32 Å, with a monoclinic angle β=93°, *b'* being the unique axis. In the austenitic setting, the martensitic axes are *a*= 6.20 Å, *b*=5.88 Å, *c* = 5.52 Å with γ=91°, *c* being the

unique axis in this setting. Upon transformation, the martensitic phase shows a polytwinned system characterized by a complex microstructure. Among all the possible martensitic twinning systems, involving {110}-type twin planes, only *a-c* twins were found in epitaxial thin films.[12,15] These types of twinning give rise to a typical microstructure, characterized by twin lamellae only oriented at 45° or at 90° with respect to the substrate plane and intersecting the surface of the film along the [110] and [100] MgO directions.[22,23] According to the nomenclature introduced in ref. 24, we will label the two different types of twinned areas as X (45°) and Y (90°) zones. These two differently twinned zones are contemporary present, as can be clearly identified in the scanning transmission electron microscopy high angle annular dark field (STEM-HAADF) images, obtained in cross **(Figure 1a**) and plan geometry (**Figure 1b**). **Figure 1c,d** reports the Fast Fourier Transforms (FFTs) of the high resolution (HR) images (Supporting Information) taken in the X and Y zones showing the involved twin planes. The two deduced twinning configurations are sketched in **Figure 1e,f**. The twinning planes involved in X-type and Y-type zones are respectively {101} and {110} in the austenitic reference. In X-type regions the twinning planes induce a flipping of the short *c-axis* from the in-plane to the out-of-plane direction switching orientation with *a-axis* only, *b-axis* remaining in the film plane. In Y-types regions, the twinning planes induce the short *c-axis* to assume two symmetric in-plane directions, corresponding approximately to the diagonal of the substrate, exchanging its orientation with *a-axis* only, *b-axis* always remaining perpendicular to the film plane. The peculiar aspect emerging from the analysis of this family of twin variants is that the twinning planes are of type-II (see Supporting Information). Out of the two possible twins found in modulated martensites and involved in MIR, type-II are characterized by the lowest twinning stress and can be activated at low values of magnetic field. [25]

The magnetic configuration and its correlation with the twin structure has been directly visualised, for the first time in ferromagnetic shape memory thin films, by means of electron

holography experiments that provide the direct evidence of the magnetic patterns inside the twinned regions. Figure 1g,h shows that the easy magnetization direction of martensite coincides with the c-axis. The easy-axis character of magnetocrystalline anisotropy was found also in 7M modulated bulk alloys.[26]The magnetic induction map of the X-type zones, observed in cross section, shows the magnetization vector (sketched by white arrows) pointing alternatively out of plane and in plane at each lamella. In the Y-type zone, observed in plan view, the magnetic vector is always in plane, switching along the two [110] directions of MgO.

The relationship between microstructure and magnetic domain structure was investigated by atomic and magnetic force microscopy (AFM/MFM) experiments (**Figure 2a, b**). AFM image (Fig 2a) shows the two regions distinguished by the different twinned structures. In X-type zones, twin planes form at the surface the typical angle of 45° with respect to the [100] MgO direction. On the other hand in Y-type zones, characterized by internal twins with twin planes running parallel to the MgO [100], the internal structure can be scarcely observed by height contrast, because of the very small surface corrugation it gives rise to.

The corresponding MFM image (Figure 2b) highlights the different magnetic configurations of the two zones. In the X-type zones, a high magnetic contrast, can be observed, consistently with the electron holography results, which show magnetization components perpendicular to the film plane. The fine details of the magnetization pointing alternatively in and out of the film plane cannot be resolved by the MFM technique. In the Y-type zones the in-plane magnetization orientation can be confirmed by the lack of any MFM signal, except for the contribution of the Bloch domain walls that display an out of plane component.

Actually, the two types of twins described before are the fine structure of larger martensitic plates as demonstrated by the large-scale SEM image of the film surface, recorded by backscattered electron detector (BSED) (**Figure 2c**). The surface of the as-grown film is composed of the two different martensitic zones mixed together in the entire area, as shown

by the bright or dark contrast. The bright plates display approximately rectangular shape with one edge several times longer than the other and aligned along the {100} directions of the substrate. A higher magnification image (**Figure 2d**) of these plates highlights the internally twinned structure, with twin lamellae of approximately 20 nm width, running along {100}-directions.

Following the previous structural analysis, the twinning in these zones is of type Y, i.e. twin planes are perpendicular to the substrate. On the other hand, plates with dark contrast exhibit twinning microstructure with lamellae that intersect the surface at 45° with respect to the edges of the substrate, relating them to (101) twinning planes, corresponding to X-zone of the TEM cross section measurements. It is noteworthy that Y-zones, in this sample, show a strong preferential orientation of the microstructure. As can be seen in Figure 2c, that is representative of the whole sample, these long plates are invariably oriented along one edge of the substrate, only. As reference we will indicate this direction as the [100] direction of the MgO, as indicated in Figure 2a-d. Such a microstructure plays a pivotal role on the anisotropic response of the film to the applied magnetic field.

In fact, as shown in **Figure 2e**, by applying the field along the [100] direction of MgO a substantial metamagnetic behavior, with a jump of magnetization outreaching 55% of the saturation value, is achieved. This jump, identified as the fingerprint of the MIR [12-14], shows here an unprecedented value. The magnetization jump ΔM=28 Am^2/Kg is achieved in a field increment of just 11 mT; the entire MIR process is completed at relatively low field (H_{max}=82 mT) and is highly reversible, the inverse process starting around 58 mT.

Another remarkable behaviour is the anisotropic character of such effect: by applying the field along the other notable directions, such as [110], or [010] of the MgO substrate, a regular magnetization curve is recorded, as can be seen in Figure 2e. The anisotropic behavior of magnetization reflects the microstructural preferential orientation of the martensitic plates, indicating that the large scale arrangement of the twinning patterns is the key element to

achieve the outstanding MIR effect that we report here. This can be proved by measuring the magnetic behaviour of other films with the same thickness but different morphologies. Two additional 200 nm thick films on 50 nm Cr have been prepared with different growth conditions giving rise to different martensitic microstructures.

The sample morphology was recorded in different areas of the samples and at different length-scales to check for the homogeneity of the microstructure all over the sample at all magnifications. By this analysis we have been able to confirm that the images we report can be considered representative of the entire films. **Figure 3** shows SEM images of the other two samples, hereafter called B and C, while we will refer to the first sample as A. Sample B has a microstructure similar to sample A, with two different X-type and Y-type zones, internally twinned in the same way as for sample A, but they are homogeneously distributed, being the Y zones equally oriented along both [100] and [010] directions of the MgO (**Figure 3a,b)**. The hysteresis loops, measured along the two [100] and [010] edges of the substrate, shows the MIR effect occurring in both directions; the jump in magnetization has almost the same value along the two directions, while its absolute value is lower than the one achieved by sample A (ΔM=15 Am^2/Kg) (**Figure 3c**). Finally, sample C shows only one kind of zone (X-type) with the very well-known 45°-type twinning, oriented in the two directions of the film plane and homogeneously mixed down to a short length scale (**Figure 3d,e**). The hysteresis loops do not show any differences between these directions and, more importantly, MIR effect has been completely suppressed (**Figure 3f**).

From these data the crucial role of microstructure in the control and substantial enhancement of the MIR effect has been demonstrated for the first time. The experimental evidence suggests that there are two key features for achieving the MIR effect in epitaxial thin films; firstly Y-type twinning regions must be present and, secondly, the field has to be applied along the long direction of the Y-regions.

In order to achieve a better understanding of the MIR effect we have performed a magnetic

field dependent MFM study of sample A. Figure 4 provides a series of images collected while applying a magnetic field along both in-plane [010] (Figure 4a,b) and [100] (Figure 4c,d) directions. While the magnetic contrast inside the X- and Y-regions changes sensitively with increasing field, the MFM images immediately show that no identifiable change in the size and distribution between the two regions occurs. It can be concluded that the MIR effect is mainly achieved by a twin variant rearrangement involving the Y-type zones.

By recalling the transmission electron holography measurements (Figure 1f), inside the Y-type regions the magnetization vectors alternate along two <110> substrate directions in a "head-to-tail" configuration, as sketched in Figure 4e. This 90° change of the magnetization direction occurs at the twin boundaries parallel to [100] MgO (i.e. parallel to the long edge of the Y-regions). On the other hand 180° domain walls are aligned along [010], that is the short edge of the Y-regions. Since [010] is the easy magnetization direction of the film (Figure 2e) in order to describe the magnetization process we can simplify the magnetic configuration by a resulting magnetic vector following the [010] direction of the substrate, as drawn in Figure 4e. By applying the magnetic field along such [010] direction the domain wall movement provides the growth of the domains inside the Y-regions aligned with the external field. Coherently, the in-field MFM images show the disappearance of the Y-regions domain walls at very low applied fields.

On the contrary, the magnetization curve along [100] direction at low field has a hard-direction character, consistently with a rotation of the resulting moment towards the applied field direction up to a critical field where the sudden jump occurs. In this case, the partial magnetization rotation gives rise to a discontinuity of the [010] magnetization component across the twin boundaries (i.e. charged twin planes) that, thanks to the low twinning stress of type–II boundaries, is at the basis of the magnetic field induced reorientation.

In conclusion, we have demonstrated that huge reversible MIR due to type-II twin boundary motion, can be obtained in a two-region martensitic thin films and its intensity and anisotropic

character can be easily controlled. Martensitic microstructure and its large scale arrangement emerge as the key elements for controlling MIR effect in ferromagnetic shape memory thin films, allowing the possibility to tune a desired response by microstructure engineering.

Experimental Section

Ni-Mn-Ga thin films of thickness of 200 nm were grown at T=350° C by r. f. sputtering at different sputtering rates, in the range 65-73 Å/min , on a 50 nm Cr (001) underlayer grown on MgO (001) at the same temperature. Ni-Mn-Ga films were deposited using a target with a composition of $Ni_{49.3}Mn_{27.8}Ga_{22.9}$ (at.%). The obtained film composition was $Ni_{53,7}Mn_{22.1}Ga_{24.2}$, as determined by energy dispersive X-ray spectroscopy (EDXS), with an uncertainty of about 0.8 at.% for each element.

The sample microstructure was studied by means of scanning electron microscopy (SEM, FEI Inspect – F) in conventional and backscattered mode. The microstructure at the nano and atomic scale was investigated by a JEOL JEM 2200FS transmission electron microscope, working at 200 kV. To perform cross-sectional transmission electron microscopy (TEM), a thin lamella has been cut from the film along the [100]-direction of the substrate using the focused-ion beam lift out technique, while for the in-plane analysis a thin foil has been prepared using dimple grinder and ion mill.

In order to study the magnetic configuration of the samples at the scale length of the martensitic twin variants, we have performed electron holography experiments. In particular, medium resolution electron holography was performed using a FEI Titan^3 microscope working at 300 kV, equipped with a spherical aberration corrector by CETCOR and fitted with a Lorentz lens and an electrostatic biprism.

Atomic force and magnetic force microscopy (AFM/MFM) images have been acquired by a Dimension 3100 microscope equipped with Nanoscope IVa controller. MFM images were

acquired in the interleave mode in zero field and by applying a magnetic field (μ_0H=75 mT) along [010] and [100] directions of MgO substrate.

Room-temperature magnetization curves have been measured by an alternating gradient force magnetometer (AGFM), applying the magnetic field in different directions of the film plane.

Supporting Information
Supporting Information is available from the Wiley Online Library or from the author.

Acknowledgements
The authors are grateful to Dr.Lara Righi (Chemistry Department of the University of Parma) for the useful discussions on martensitic structures.
The financial support from the 2007–2013 FESR Operative program of the Emilia Romagna Region(Activity I.1.1) is acknowledged.

Received: ((will be filled in by the editorial staff))
Revised: ((will be filled in by the editorial staff))
Published online: ((will be filled in by the editorial staff))

[1] M. Acet, L. Mañosa, and A. Planes, in *Handbook of Magnetic Materials,* Vol. 19 (Ed. K. H. J. Buschow), North-Holland, Amsterdam, The Netherdlands, **2011,** pp. 231-283.

[2] R. Kainuma, Y. Imano, W. Ito, Y. Sutou, H. Morito, S. Okamoto, O. Kitakami, K. Oikawa, A. Fujita, T. Kanomata, K. Ishida, *Nature* **2006**, *439*, 957.

[3] J. Liu, T. Gottschall, K. P. Skokov, J. D. Moore, O. Gutfleisch, *Nature Mater.* **2012**, *11*, 623.

[4] L. Mañosa, D. Gonzalez-Alonso, A. Planes, E. Bonnot, M.Barrio, J. L. Tamarit, S. Aksoy,

M. Acet, *Nature Mate*r. **2010**, *9*, 478.

[5] M. Gueltig, H. Ossmer, M. Ohtsuka, H. Miki, K. Tsuchiya, T. Takagi, M. Kohl, *Adv. Energy Mater.* **2014**, *4*, 1400751.

[6] D. C. Dunand, P. Müllner, *Adv. Mater.* **2011**, *23*, 216.

[7] M. Thomas, O. Heczko, J. Buschbeck, Y. W. Lai, J. McCord, S. Kaufmann, L. Schultz, S. Fähler, *Adv. Mat.* **2009**, *21*, 3708.

[8] I. Aaltio, A. Soroka, Y. Ge, , O. Soderberg, S.P. Hannula, *Smart materials and struct.* **2010**, *19*, 075014.

[9] K. Bhattacharia, R. D. James, *Science* **2005**, *307*, 53.

[10] K. Ullakko, J. K. Haung, C. Kanter, R. C. O'Handley, V. V. Kokorin, *Appl. Phys. Lett.* **1996**, *69*, 1966.

[11] A. Sozinov, N. Lanska, A. Soroka, W. Zou, *Appl. Phys. Lett.* **2013**, *102*, 021902.

[12] M. Thomas, O. Heczko, J. Buschbeck, U. K. Rößler, J. McCord, N. Scheerbaum, L. Schultz, S. Fähler, *New J. Phys.* **2008**, *10*, 023040.

[13] O. Heczko, M. Thomas, J. Buschbeck, L. Schultz, S. Fähler, *Appl. Phys. Lett.* **2008**, *92*, 072502.

[14] Y. Zhang, R. A. Hughes, J. F. Britten, J. S. Preston, G. A. Botton, M. Niewczas, *Phys. Rev. B* **2010**, *81*, 054406.

[15] T. Eichhorn, R Hausmanns, G. Jakob, *Acta Mater.* **2011**, *59*, 5067.

[16] C. A. Jenkins, R. Ramesh, M. Huth, T. Eichhorn, P. Pörsch, H. J. Elmers, G. Jakob, *Appl. Phys. Lett.* **2008**, *93*, 234101.

[17] A. Backen, S. R. Yeduru, M. Kohl, S. Baunack, A. Diestel, B. Holzapfel, L. Schultz, S. Fähler, *Acta Mater.* **2010**, *58*, 3415.

[18] P. Ranzieri, S. Fabbrici, L. Nasi, L. Righi, F. Casoli, V. A. Chernenko, E. Villa, F. Albertini, *Acta Mater.* **2013,** *61*, 263.

[19] Y. Luo, P. Leicht, A. Laptev, M. Fonin, U. Rüdiger, M. Laufenberg, K. Samwer, *New J. Phys.* **2011**, *13*, 013042.

[20] J. Tillier, D. Bourgault, P. Odier, L. Ortega, S. Pairis, O. Fruchart, N. Caillault, L. Carbone, *Acta Mater*. **2011**, *59*, 75.

[21] L. Righi, F. Albertini, E. Villa, A. Paoluzi, G. Calestani, V. Chernenko, S. Besseghini, C. Ritter, F. Passaretti, *Acta Mater*. **2008**, *56*, 4529.

[22] S. Kaufmann, R. Niemann, T. Thersleff, U. K. Rößler, O. Heczko, J. Buschbeck, B. Holzapfel, L. Schultz, S. Fähler, *New J. Phys.* **2011**, *13*, 053029.

[23] B. Yang, Z. B. Li, Y. D. Zhang, G. W. Qin, C. Esling, O. Perroud, X. Zhao, L. Zuo, *Acta Mater*. **2013**, *61*, 6809.

[24] A. Diestel, V. Neu, A. Backen, L. Schultz, S. Fähler, *J. Phys. : Condens. Matter* **2013**, *25*, 266002.

[25] L. Straka, A. Soroka, H.Seiner, H. Hänninen; A. Sozinov, *Scripta Mater*. **2012**, *67*, 25.

[26] F. Albertini, M. Solzi, A. Paoluzi, L. Righi, in: *Materials Science Forum* vol. 583 (Ed:V. A. Chernenko) *Vol. 583*, Trans Tech Publications, Switzerland **2008**, pp.169-196.

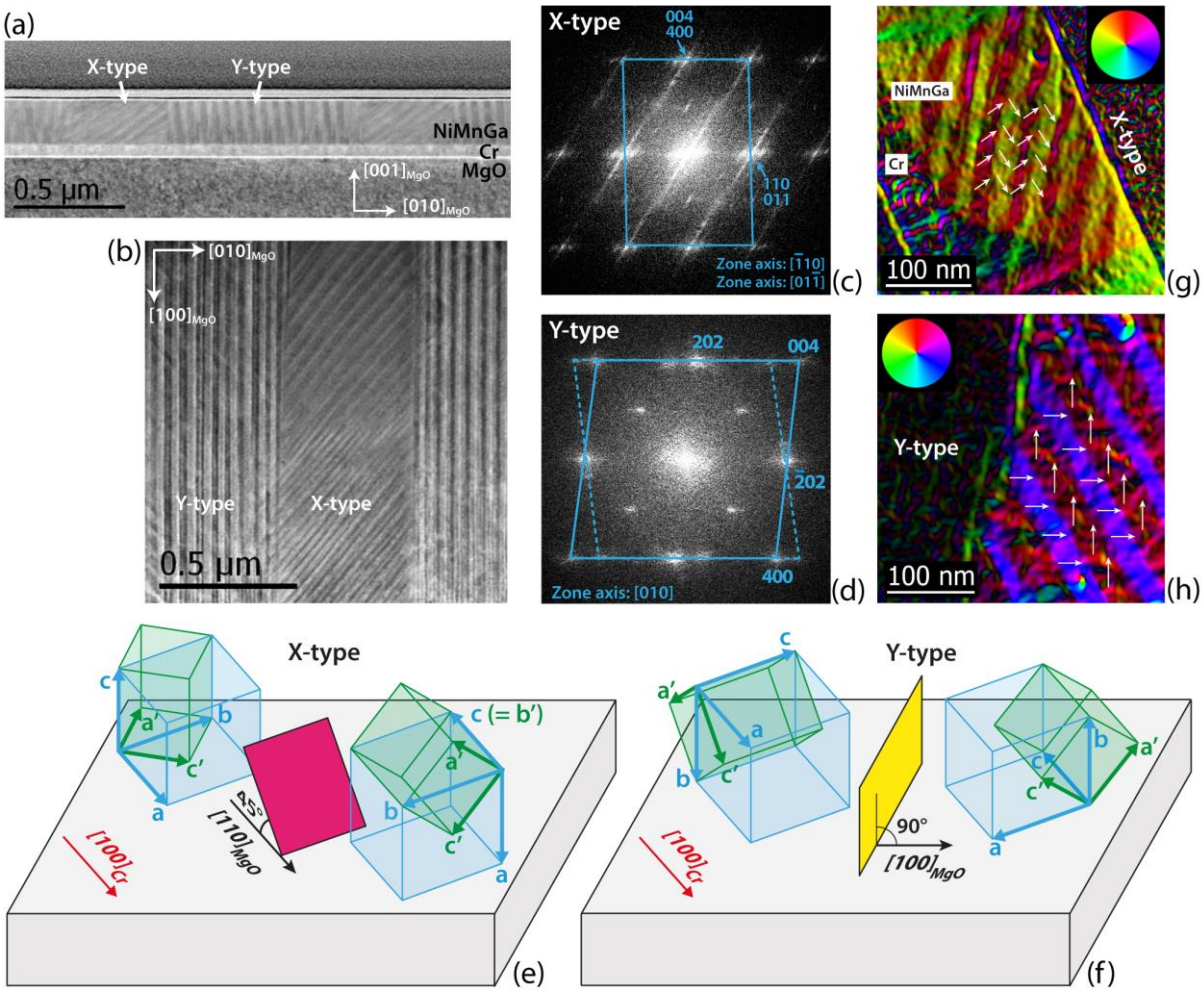

Figure1. a), b) STEM-HAADF images obtained in cross section and plan view. c), d) FFTs of the high resolution images (supplementary information) taken in the X- and Y-type zones. e), f) Sketches of the two different twinning configurations. g), h) Magnetic induction colour maps obtained by electron holography for X and Y-type zones, taken in cross section and plan view, respectively. The colours indicate the magnetization direction, as schetched by white arrows, while the colour saturation is related to the magnetization intensity.

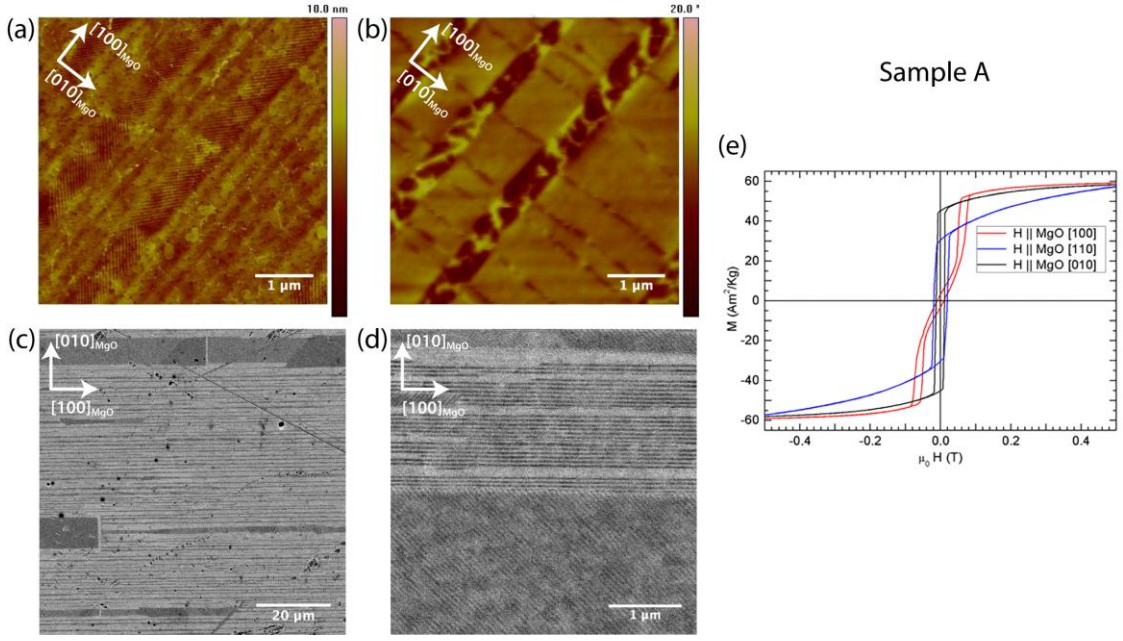

Figure 2. Microstructure, magnetic domain structure and magnetization processes of the sample A. a) AFM and b) MFM. c) SEM image on large scale and d) magnification of a 5x5 μ^2 area. e) Hysteresis loops measured by applying the magnetic field along different directions in the film plane.

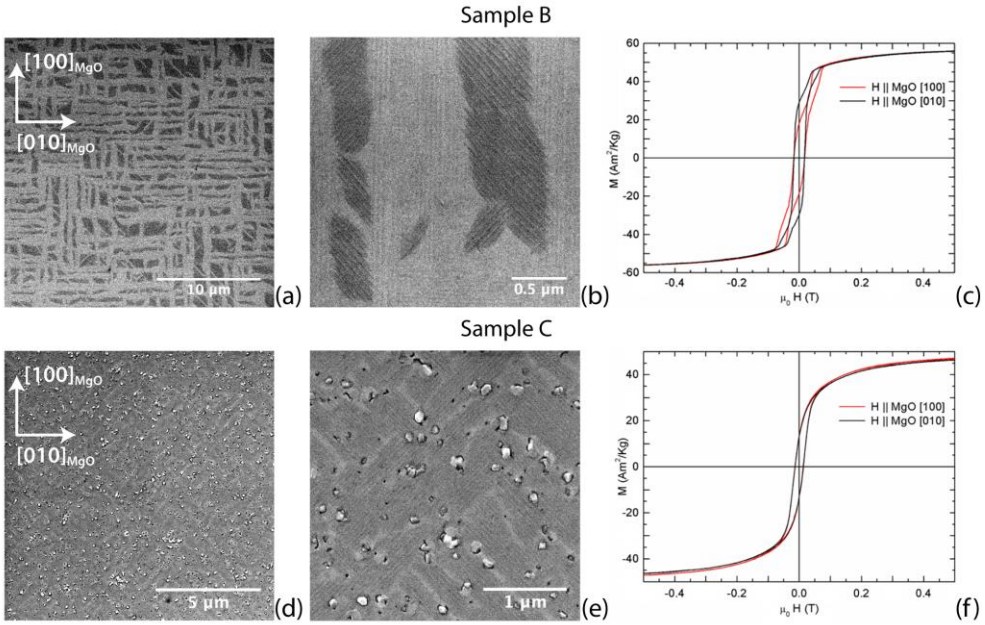

Figure 3. Microstructure, magnetic domain structure and magnetization processes of sample B (top row) and sample C (bottom row). a), d) SEM on large scale and b), e) magnification of

a 5x5 μ^2 area. c), f) Hysteresis loops measured by applying the magnetic field along different directions in the film plane.

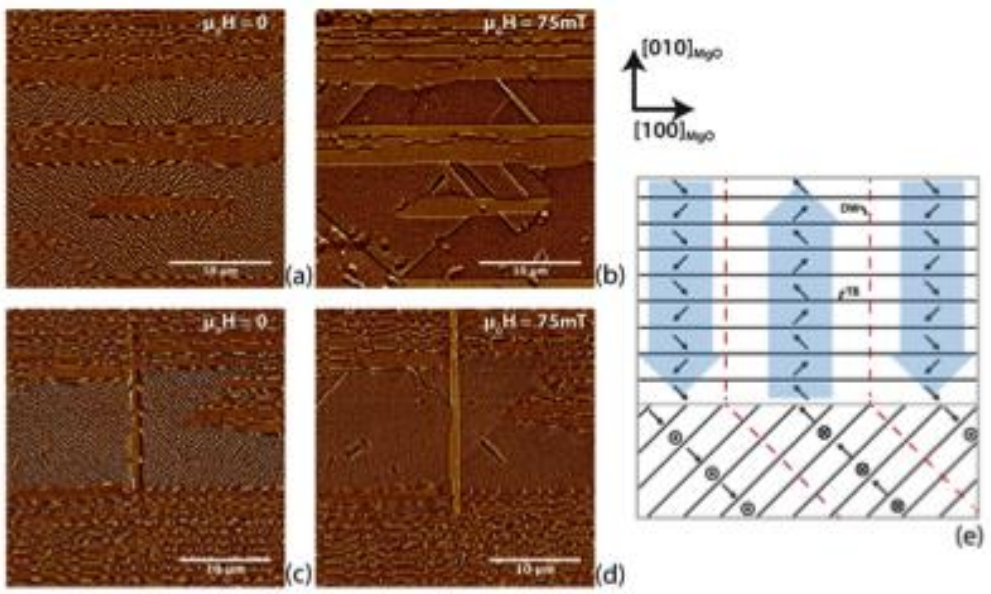

Figure 4. Magnetic field dependent MFM study carried out by applying a magnetic field along [010] direction a), b) and [100] direction c), d). f) Schematic sketch of the magnetic configuration in X-type (bottom) and Y-type (top) zones. DW:180° domain walls (red dashed lines), TB: type-II twin boundaries (black full lines). The superimposed blue arrows represent the resulting magnetic vectors along [010] MgO direction.

The table of contents entry should be 50−60 words long, and the first phrase should be bold.

Giant magnetically induced twin variant reorientation, comparable in intensity with bulk single crystals, was obtained in epitaxial magnetic shape memory thin films. It was found to be tunable in intensity and spatial response by the fine control of microstructural patterns at the nanoscopic and microscopic scale. A thorough experimental study (including

electron holography) has allowed a multiscale comprehension of the phenomenon.

Keyword
ferromagnetic shape memory thin films, magnetically induced twin variant reorientation, martensitic microstructure, electron holography, multifunctional magnetic materials

*Paolo Ranzieri, Marco Campanini, Simone Fabbrici, Lucia Nasi, Francesca Casoli, Riccardo Cabassi, Vincenzo Grillo, Cesar Magén, Federica Celegato, Gabriele Barrera, Paola Tiberto, Franca Albertini**

Title
Achieving giant magnetically induced reorientation of martensitic variants in magnetic shape memory Ni-Mn-Ga films by microstructure engineering

ToC figure ((Please choose one size: 55 mm broad × 50 mm high **or** 110 mm broad × 20 mm high. Please do not use any other dimensions))

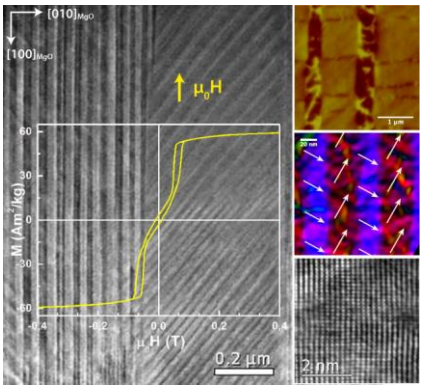

Supporting Information

Achieving giant magnetically induced reorientation of martensitic variants in magnetic shape memory Ni-Mn-Ga films by microstructure engineering

*Paolo Ranzieri, Marco Campanini, Simone Fabbrici, Lucia Nasi, Francesca Casoli, Riccardo Cabassi, Vincenzo Grillo, Cesar Magén, Federica Celegato, Gabriele Barrera, Paola Tiberto, Franca Albertini**

1. Electrical measurements

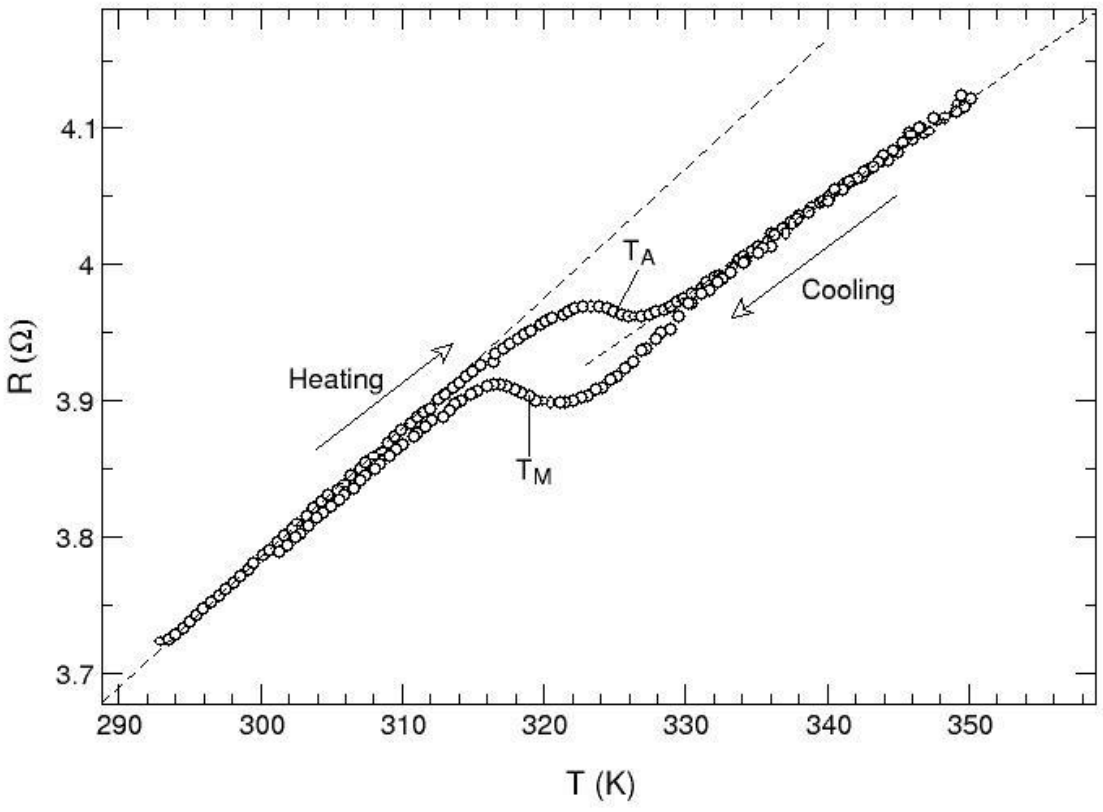

Figure S1. Resistance as a function of temperature of sample A. The dashed lines indicate the slope below and above the transition.

The transformation behaviour was characterized by the temperature dependence of the electrical resistance determined by the four-probe method. It is well known that the electrical resistance of Heusler alloys has a metallic character: it increases by increasing temperature. At the Curie transition, a decrease of slope is expected by increasing temperature, while at the martensitic transformation an abrupt change of intensity together with a thermal hysteresis between the heating and cooling curves are expected.[18] The results of electrical measurements are shown in **Figure S1** where only one transition, characterized by hysteresis, is present. This behaviour can be attributed to the merging of the aforementioned martensitic and Curie transitions, resulting in a first-order transition between a ferromagnetic martensite and a paramagnetic austenite, as found in several bulk materials of similar composition.[26] The transformation temperatures on heating and cooling are T_A=325 K and T_M=319 K respectively. The slope in the martensitic state (i.e. below the transition) is greater than in the austenitic state (i.e. above the transition).

2. TEM characterization of the twinning configuration

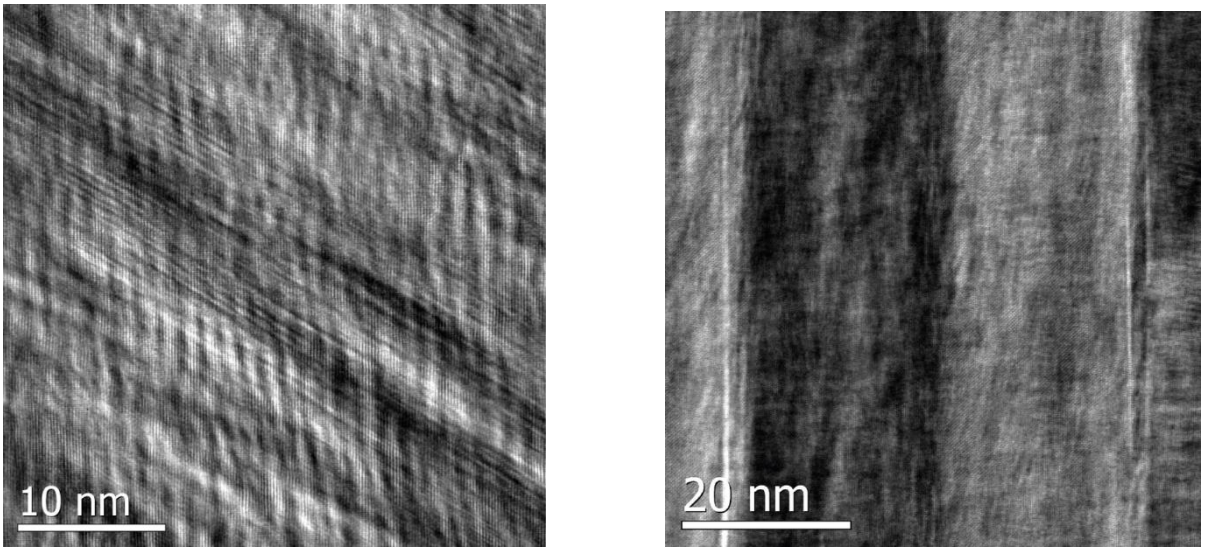

a) b)

Figure S2.

a) HRTEM cross sectional image taken in the X region b) HRTEM plan view image taken in the Y zones, showing the twin planes involved inside the two zones. The FFTs of the two images are shown in Figure 1c and 1d, respectively.

The peculiar aspect emerging from the analysis of twin variants in the Y-type regions is that the twinning plane, described as {101} in austenitic reference, is a type-II twinning plane characterized by irrational indices. The experimental proof is provided by the following HREM images and corresponding FFTs.

In **Figure S3** and **Figure S4** two HREM images of the twin variants of the Y region are shown in cross-sectional and planar view, respectively. The zooms of the rectangular areas across the twin boundaries, indicated in the figures by the white dashed square, are superimposed to the images.

Since the two twinned crystals in type-II twin boundaries are related by a rotation of π around the η1 axis, the diffraction pattern acquired orienting the sample along the η1 direction must display only a single pattern; this is indeed verified in the in cross-sectional view (**Figure S3a**) and related FFT (**Figure S3b)**, where only a single diffraction pattern is observed along the [101] direction. A scheme of the twinning elements in this projection is given in **Figure S3c)**.

It is worth to note that even in the enlargement of the HREM image in Figure S3a) a clear continuity of the atomic planes across the twin boundaries is visible, proving that in this zone axis the twinned crystal is perfectly generated by a rotation of one twin variant of an angle π around the twinning direction.

The complementary geometry can be explored in planar view: the FFT (**Figure S4b**) of the HREM image view (**Figure S4a**) shows that, if the sample is oriented along a zone axis perpendicular to the twinning direction, a mirror plane normal to η1 is observed in reciprocal lattice. A scheme of the twinning elements in this projection is given in Figure S4c). The enlargement of the twin boundary reported in Figure S4a) also highlights how in HREM observations along an axis that differs from the twinning direction an overlap of the twinning crystals in is unavoidable at the type-II twin interface, because of an irrational K1 plane.

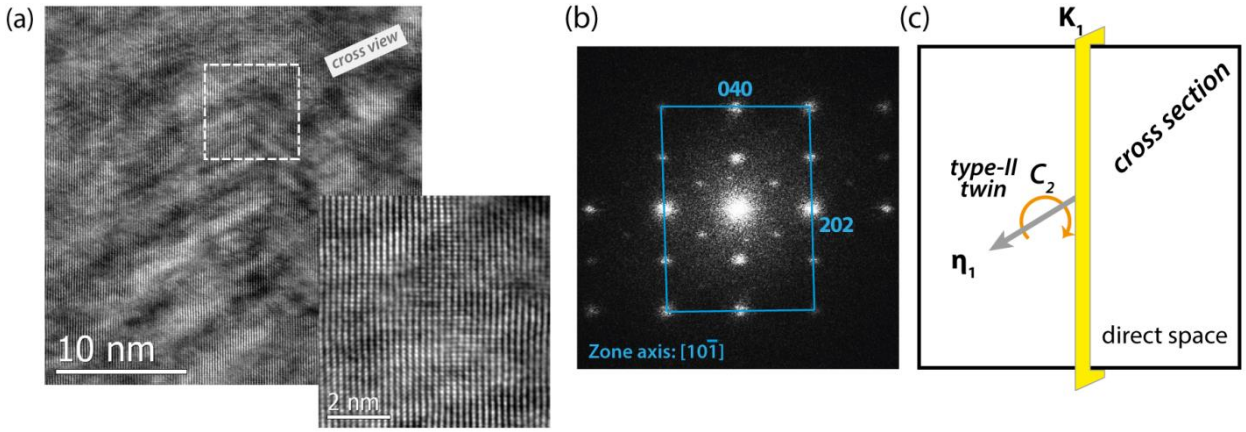

Fig. S3.

a) HREM images of 90° lamellae in cross-sectional view. An enlargement of the square area (marked by the dashed line) across the twinning plane is given. b) FFT of the HREM image; no noticeable effect of the twin is visible in this projection. c) Schematic representations of the typical twinning elements characterizing a type-II twin in the direct space, when observed along the twinning direction η_1.

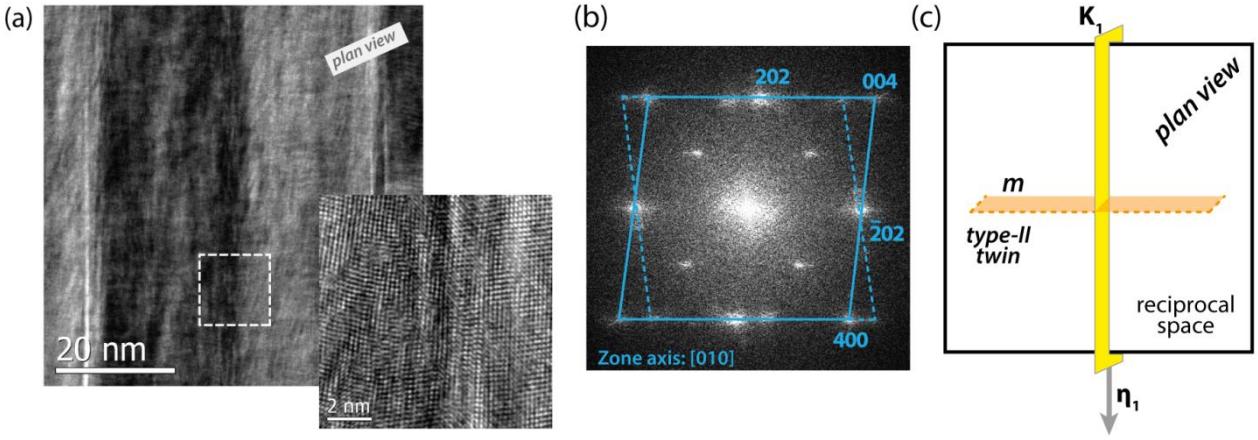

Figure S4.

a) HREM images of 90° lamellae in planar view. An enlargement of the square area (marked by the dashed line) across the twinning plane is given. b) FFT of the HREM image; a clear effect of the twin is visible in this projection. c) Schematic representations of the typical twinning elements characterizing a type-II twin in the reciprocal space, when observed along a direction normal to the twinning direction η_1.

Click here to download Supporting Information: supporting_information_ranzieri_albertini.docx